CHAPTER 3

Studies on adsorptive removal of fluoride using CeO_2/BC

3.1. INTRODUCTION

This chapter deals with the removal of fluoride from drinking water using CeO_2/BC. Fluoride (F^-) is widely present in the natural world, yet it negatively affects people [155]. Low amounts of F^- are crucial micronutrients for bone formation [156]. However, prolonged exposure to high F^- levels can seriously endanger human health [157]. Toxic effects from excessive human consumption include skeletal abnormalities, bone thinning, dental fluorosis, and Alzheimer's [28,158]. Biotite, cryolite, topaz, fluorite, fluorapatite, and muscovite are fluoride-containing minerals that naturally leach fluoride when it rains, contaminating groundwater and surface water. [118,159]. Fluoride pollution is a problem that has caused concern in many regions of the world. According to data, high-fluoride-laden water is used by more than two hundred million people in over 30 countries [160,161]. The World Health Organization states that to safeguard human health from the harmful effects of F^-, the concentration of F^- in drinking water should not exceed 1.5 mg/L [41].

A number of methods, including precipitation [162], ion exchange [163], electrodialysis [164], and adsorption [165–167] can be used to defluoridate water and wastewater. It should be noted that every approach has distinct benefits and downsides [168,169]. Adsorption stands out among them as a potential defluoridation technology owing to its low- cost, flexible operational conditions, and appreciable removal efficacy for pollutants with low concentrations [170–175]. Graphene oxide [176], carbon nanotubes, bone char, and activated carbon are some examples of efficient adsorbents with attributes like significant surface area. Metals like Al, Mg [177], Zr, La, Fe and rare earth metals are used for developing efficient de-fluoridating material or modifying surfaces. Among them, some metals like aluminium may cause secondary pollution in water due to release of aluminium ions in water. Aluminium pollution has been proposed as a trigger for the development or advancement of Alzheimer's disease in humans (WHO 2003).

Rare earth oxides are recognised as effective materials for fluoride removal [178]. Many researchers have confirmed that Cerium has a particular affinity for fluoride over a broad pH range as it is highly insoluble in water [179–181]. Some Effective fluoride adsorbents include Fe-Al-Ce tri-metal oxide adsorbent [182], binary hybrid AlCe oxide [183], CeO_2 nanorods [184], and CeO_2 [185] Cerium alginate crosslinked biochar [186] HAp-Ce metal organic framework [187].

Biochar has a large surface area, pore volume, and surface functional groups and excellent ion exchange properties. These properties make it an ideal choice for the purification of water [188]. This biochar can be modified pre- and post-treatment using different inorganic/organic salts, acids, etc. Throughout its life cycle, "it has the ability to cut greenhouse gas emissions by around 870 kg of CO_2 equivalent per tonne of dry feedstock" [189]. According to Tangsir et al. [190], sugarcane bagasse, a significant biomass waste, is produced in sugarcane industries in countries like Brazil, Mexico, India, and China for the production of sugar and alcohol Lignin, cellulose, and hemicellulose present in bagasse make it the perfect raw material for the production of biochar [191,192].

Due to high cost of rare earth metals and block-bodied shape [179] limit their practical usage. Combining Cerium with expensive cross-linking agents also increases its production cost. To address these issues, low-cost, easily available materials incorporating Cerium with facile recyclability are in critical demand for expanding their commercial use as a de fluoridating agent.

Thus, our aim was to develop a new adsorbent by simply precipitating cerium oxide onto the porous sugarcane bagasse biochar's surface, which was then tested in the adsorptive removal of F^- from wastewater. The suggested approach is innovative and more practicable for developing cerium oxide due to the non-sintering technique that avoids the need for high temperatures for calcining with straightforward mechanisation. Our approach for developing

cerium-incorporated adsorbent is novel in the sense that it does not use any expensive cross-linkers and modifies biochar by post-treatment. The use of biochar as a precursor for the adsorbent also makes this approach environmentally friendly. This method has the potential to provide a cost-effective and sustainable solution for removing fluoride from water.

3.2. METHODOLOGY AND EXPERIMENTAL

3.2.1 Preparation of CeO_2-loaded biochar

Biochar (BC) was prepared by pyrolyzing Sugarcane bagasse, and its detailed procedure is given in chapter 2 (section 2.3). The required amount of Ammonium Cerium (IV) Nitrate was dissolved distinctly in de-ionized water and this solution is stirred for 60 minutes at 40 ºC. At the same time, a definite amount of biochar was dissolved in another beaker and stirred for 60 minutes at 40 ºC. After this, both the solutions were mixed and kept under stirring at 60 ºC. Ammonia solution (ammonium hydroxide) was added dropwise to the stirring solution until the pH reached 12. The obtained precipitated solution was kept overnight to promote the precipitate's selective development. The precipitate was filtered and rinsed seven times with de-ionized water, followed by three times by ethanol to get rid of impurities. The resultant product was subjected in a hot air oven at 80 ºC for twelve hours, taken out and ground to get CeO_2-modified biochar (CeO_2/BC). Cerium-free biochar was pristine biochar (BC).

3.2.2 Characterization of CeO_2/BC

The synthesis of CeO_2/BC and its physical as well as chemical properties were characterized with different characterization tools such as FTIR, XPS, SEM, EDAX, XRD, BET and pHzpc measurement.

3.2.3 Fluoride batch adsorption experiments

Batch experiments were executed in triplicate in a 250 mL Beaker to assess the impact of various regulatory parameters (adsorbent dose, pH, contact time, counter anions (HCO_3^-, SO_4^{2-}, NO_3^-, Cl^- and initial fluoride concentration). To evaluate the adsorption capacity of unmodified biochar, CeO_2, and CeO_2/BC for fluoride, a pre-adsorption experiment was conducted. The experimental conditions consisted of an initial fluoride concentration of 10 mg/L, a dose of 3 g/L, pH level at 7 ± 0.3, and a duration of 360 minutes. Subsequently, fluoride adsorption tests were performed using different amounts of CeO-loaded biochar under similar experimental conditions as mentioned above. By increasing the adsorbent dose from 0.1 g/L to 3 g/L, the effect of adsorbent dose on fluoride adsorption was examined. The impact of contact time was investigated with an initial fluoride concentration of 10, 20, and 30 mg/L and an adsorbent dosage of 3 g/L. The samples were centrifuged, and residual fluoride concentrations were calculated at a predetermined interval of time. Using solutions with various fluoride concentrations ranging from 5 mg/L to 30 mg/L, the effects of initial fluoride concentration were investigated. The influence of pH was examined by varying the pH of the solution from 2 to 10. At different contact times (30-360 min).

3.2.4 Reusability test of synthesized adsorbent

To ascertain whether the adsorbent could be reused, 0.075 g of used CeO_2/BC adsorbent after fluoride (10 mg/L) adsorption was contacted with 25 mL of 0.5 M NaOH solution. and agitated for 60 minutes at 200 rpm. Following desorption, the adsorbent is collected and properly washed with de-ionized water to remove NaOH completely and used for next cycle of adsorption (F^- = 10 mg/L, pH =7, contact time = 120 minutes). Under the same experimental conditions, the recyclability test was performed three times, and the adsorption capacity for each cycle was determined.

3.3. BIOCHAR SAMPLE CHARACTERISATION

3.3.1. SEM and EDAX analysis

Using scanning electron micrographs, it can be seen that the pyrolysis of biomass led to the production of cracks on the raw biochar's surface. These cracks were brought about by releasing volatile organic matter from the breakdown of lignocellulosic matrix components, improving porosity. SEM micrographs demonstrate a honeycomb-like structure, indicating that the sugarcane biomass's carbonaceous skeleton is preserved even after pyrolysis Fig 3.1(a) and (b) [193]. After incorporating cerium on biochar via precipitation we observed that pores have become larger and surface comparatively smoother than raw biochar. Upon anchoring cerium (Ce) onto the surface of raw biochar, there is a noticeable improvement in the smoothness of the biochar's surfaces in comparison to the pristine biochar (as shown in Fig. 3.1(c) and (d)). This phenomenon leads to a gradual reduction in the specific surface area of the resulting CeO_2/BC, a change verified by the BET analysis results.

Furthermore, it is evident that there is a well-dispersed presence of small micro-sized cerium oxide crystals that are partially integrated within the biochar pores and partially agglomerated on the original biochar surface. This mechanical bonding, likely due to the embedding of cerium, could be a contributing factor to the observed decrease in the surface area of the modified biochar.

It was determined that the elements C, Ce, and O are present in appropriate levels based on their atomic and weight percentages from the elemental compositions and characteristics peak of Cerium, Carbon and Oxygen. Therefore, EDAX reports proved that the CeO_2/Biochar was successfully made. Following adsorption, the SEM micrographs exhibit distortion on the surface of biochar. This phenomenon is believed to be either caused by complex formation

between Cerium and fluoride ions or electrostatic interactions that occur between negatively charged fluoride ions and positively charged biochar surface resulting from the presence of Cerium on its surface. The interaction between fluoride ions and these surface charges can lead to changes in charge distribution and surface energy, ultimately leading to the observed distortion Fig 3.1(e) and (f).

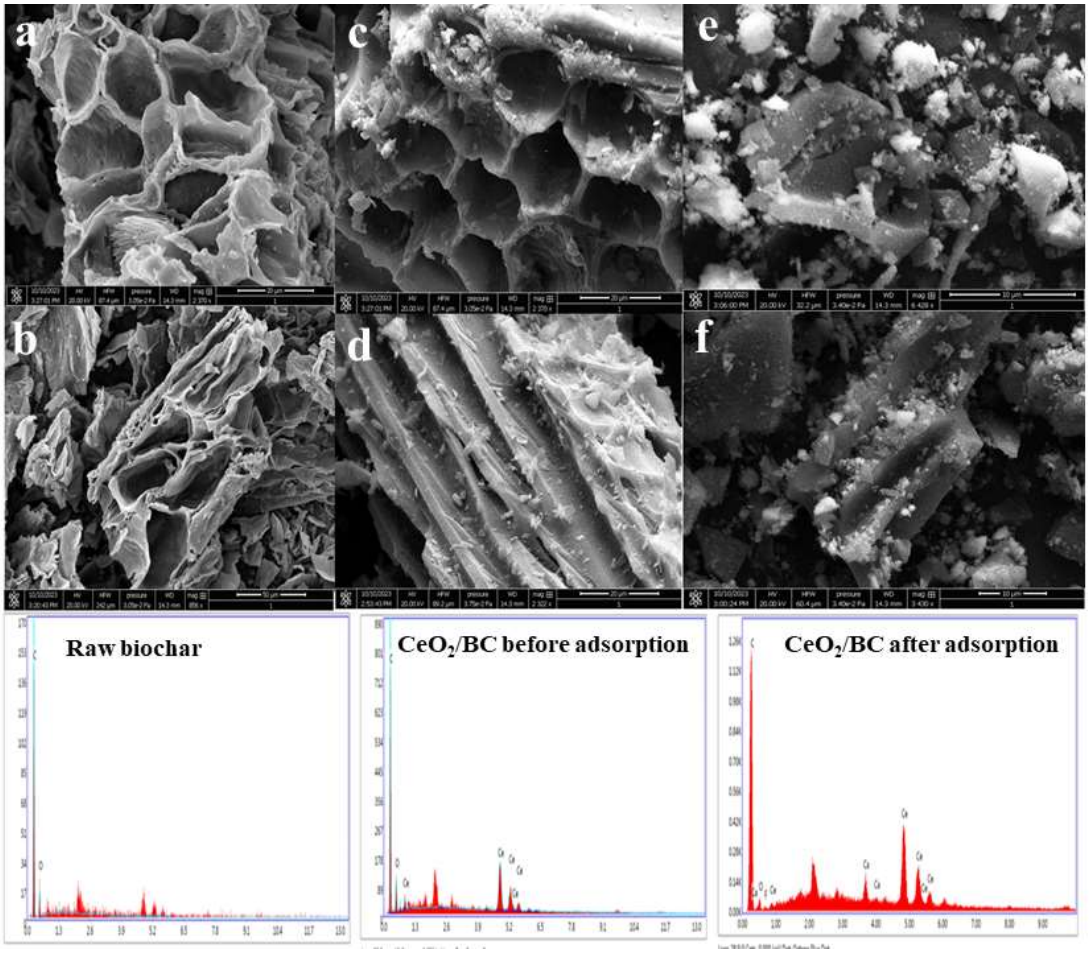

Fig. 3.1 SEM-EDAX of Raw biochar (a and b): CeO_2/BC (c and d) before adsorption; (e and f) after adsorption

3.3.2. XRD analysis

As one of the dependable approaches for determining a compound's crystalline structure and phase, X-ray diffraction patterns were examined for both pristine and Cerium-modified

biochar. The diffraction peaks of Cerium-modified biochar were well indexed with CeO_2 (JCPDS File no. 34-0394), showing the crystalline nature of the adsorbent with its peaks at 2θ 28.53º, 33º, 47.5º, 56.26º corresponding to miller indices (111), (200), (220) and (311) respectively. Synthesised biochar is in an amorphous state with peaks ranging from 2θ (20° to 30°) matching with the stacking structure of aromatic layers of graphite (graphite 002) Fig. 3.2(a). Biochar has distinct, unlabeled peaks that are indicative of several inorganic components. Comparable results were stated by Liu et al. [194].

3.3.3. BET analysis

BET analysis shows that obtained isotherms of both materials are consistent with type IV isotherms having H2 hysteresis loop, which suggests that the materials were produced with mesoporous properties [195] and they have pores with wide bodies and narrow necks [196] Fig. 3.2(b). The occurrence of capillary condensation within the mesopores is indicated by the open hysteresis loop observed in the BET isotherms of both types of biochar. Smaller pores may trap gas molecules due to the cohesive forces of the liquid phase of the adsorbate, resulting in delayed desorption during the desorption branch of the isotherm, thus displaying as the open loop [196]. Raw biochar was found to have a specific surface area equals to 277 m^2/g, a pore volume of 0.12 cm^3/g, and an average pore diameter of 2.41 nm. A decrease in surface area to 260.05 m^2/g was observed upon the modification of biochar with Cerium. This reduction can be attributed to the incorporation of Cerium within the pores of the raw biochar. Additionally, a slight increase in both pore volume and pore diameter was observed in the Cerium-modified biochar. This increase may be ascribed to the chemical precipitation process inherent to the modification process, potentially leading to the formation of new pores or the interconnection of previously isolated pores, possibly induced by thermal treatment. The pore volume and

average pore diameter of modified biochar are 0.21 cm^3/ g and 3.21 nm, respectively as shown in Table 3.1.

Table 3.1: Comparing values of surface area, pore volume and pore size of synthesized CeO_2/ BC and Raw biochar

Sample description	BET surface area (m^2/g)	BJH average pore size (nm)	BJH pore volume (cm^3/g)
CeO_2/BC	260.05	3.21	0.21
Raw Biochar	277	2.41	0.12

3.3.4. FTIR analysis

Fig. 3.2(c) represents FTIR spectra of raw biochar, CeO_2/BC before and after adsorption experiment. The O-H stretching vibration ascribes a broad adsorption peak at 3417 cm^{-1} [197]. Low intensity bands at 2923 cm^{-1} and 2853 cm^{-1} signify C-H asymmetric stretching and C-H symmetric stretching, respectively. The 1633 cm^{-1} peak might result from O-H bending vibrations [198]. The peak at 1052 cm^{-1} shows the presence of C-O band [197]. The infrared spectral fingerprint region is in the 1000-400 cm^{-1}. The characteristic peak confirms the presence of CeO_2 nanoparticles at 665 cm^{-1}, which corresponds to the O-Ce-O band [199–201]. Based on the findings, it can be deduced that the raw biochar was effectively modified with Ce while retaining all of the functional groups present in sugarcane biochar. Upon adsorption, no significant changes were observed in the spectra compared to before adsorption. However,

there was a notable decrease in the intensity of the O-Ce-O peak, suggesting that cerium oxide plays a role in fluoride removal by forming complexes.

3.3.5. pH_{PZC} analysis of CeO_2/BC

Our adsorbent CeO_2/BC has a net point of zero charge at pH equal to 7 obtained by salt addition method Fig. 3.2(d) and 7.17 by Zeta analysis Fig 3.2 (e). Due to protonation, the net charge on the surface of the adsorbent is positive when the solution's pH is below pH_{PZC}. Due to electrostatic force, this condition favour's the adsorption of anions on the adsorbent's surface [202]. Above pH 7, due to deprotonation adsorbent's surface becomes negatively charged.

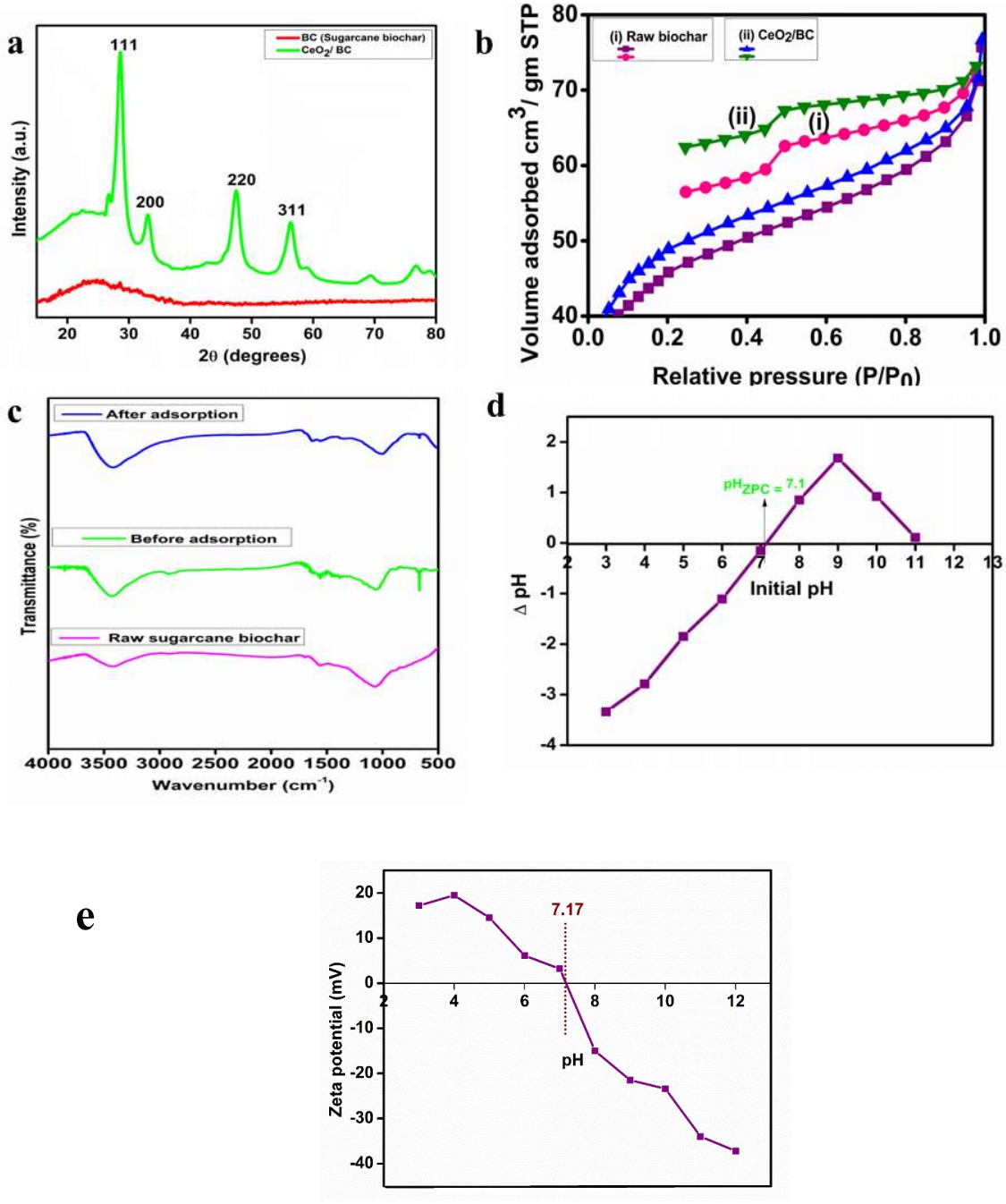

Fig. 3.2 (a) XRD diffractograms of sugarcane biochar and CeO_2/BC; (b) N_2 adsorption-desorption isotherms; (c) FT-IR spectrum of CeO_2/BC before and after adsorption; (d) pHzpc of CeO_2/BC; (e) Zeta potential of CeO_2/BC

3.4 BATCH ADSORPTION STUDIES

3.4.1 Pre adsorption test and Effect of cerium loading on adsorption

During the pre-adsorption experiment, it was observed that fluoride removal rates for unmodified biochar, CeO_2, and CeO_2/BC were 10%, 16%, and 58%, respectively Fig. 3.3(a). These findings demonstrate that incorporating Cerium into pristine biochar significantly enhances its F^- ion capture capability, with the highest adsorption capacity observed by CeO_2/BC. For instance, as the loading of cerium oxide on pristine sugarcane biochar increased, fluoride removal also increased. Specifically, increasing the cerium oxide loading from 5% to 10% resulted in a 71% increase in F^- removal. However, further increasing cerium loading did not lead to a substantial increase in fluoride removal Fig. 3.3 (b). Consequently, subsequent experiments were exclusively conducted using CeO_2/BC with a 10% loading of Cerium.

3.4.2 Effect of optimum adsorbent dose on fluoride adsorption

The effect of synthesised adsorbent dose on fluoride removal using CeO_2/BC is shown in Fig. 3.3(c). Because pristine/ unmodified biochar adsorbs negligible fluoride, the effect of dose was investigated using only designed biochar. It was discovered that increasing the dose from 1 g/L to 2.2 g/L F^- sorption rose from 60% to 86.9% for Cerium oxide-loaded biochar, but further increase in dose up to 3 g/L had a slight effect on sorption percentage. So, a sorbent dose of 3 g/L of CeO_2/BC was found to be appropriate for removing fluoride from water. Fig. 3.3 (c) illustrates clearly that the optimum dose significantly affects fluoride removal using CeO_2/BC. It can be concluded that CeO_2/BC is an efficient and practical material to be used for defluoridation purposes of water.

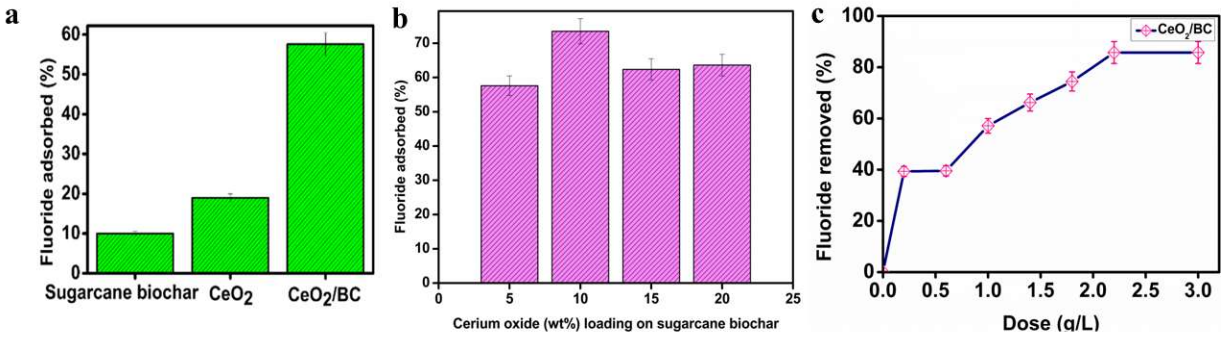

Fig. 3.3 (a) Pre-adsorption test results; (b) Effect of cerium oxide loading % on biochar for fluoride uptake; (c) Effect of adsorbent dose

3.4.3 Effect of initial pH of solution on fluoride adsorption

The results of the pH study are presented in Fig. 3.4 (a). It was observed that at lower pH values of 2 and 3, the ability to remove fluoride is significantly weaker. This may be attributed to the formation of hydrofluoric acid, which reduces the availability of fluoride ions [203]. The removal percentage of fluoride was found to be highest at pH 4, with a value of 82.78%. However, as we moved from acidic to basic conditions (pHs ranging from 4 to10), the removal percentage decreased to approximately 59%. Additionally, the sorption capacity also decreased up to 3 mg/g at pH 10. These findings suggest that electrostatic forces between CeO_2/BC and F^- play a crucial role in fluoride removal and align with CeO_2/BC's pH_{zpc} value measured at pH 7. It is known that the pH of the solution dramatically influences the nature of electrostatic forces between adsorbent and adsorbate, affecting sorption performance.

3.4.4 Effect of counterions on CeO_2/BC

The influence of bicarbonate, sulphate, chloride, and nitrate on the removal of fluoride by CeO_2/BC is depicted in Fig. 3.4 (b). The figure shows that although the presence and increment of all three anions reduce the ability of biochar to eliminate fluoride to a certain

degree, the effect of bicarbonate is more severe (approximately 40% for 10 mg/L and 35% for 50 mg/l) than that of nitrate (about 70%) and sulphate (62%). This is brought on by the increase in pH of the solution caused by the OH ion's dissolution in the sample [204,205]. As demonstrated by pH_{zpc} and the effect of pH, the pH of the solution affects the adsorbent's performance. This increase in pH also affects the adsorption of F^- by biochar because of the decreasing strength of electrostatic forces between adsorbent and adsorbate.

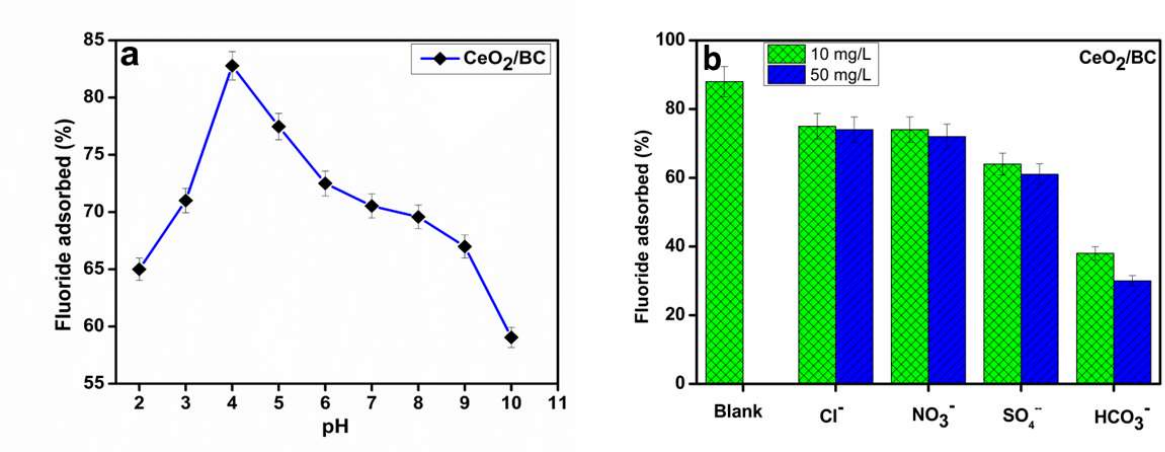

Fig. 3.4 (a) Effect of initial pH on fluoride removal percentage of CeO_2/BC; (b) effect of Counterions

3.4.5 Effect of contact time on adsorption

It is evident that the rate of F^- adsorption significantly increases for the first 30 minutes and gradually decreases afterwards, reaching equilibrium. Within 30 minutes, 69% of the fluoride was adsorbed, and equilibrium was achieved in 360 minutes with 74% fluoride adsorption Fig. 3.5 (a). In the early stages of the process, a high affinity for fluoride ions is exhibited by the cerium-modified biochar, resulting in the rapid adsorption kinetics observed. This rapid uptake is attributed to the abundance of accessible active sites on the surface of the adsorbent, where

fluoride ions can readily bind due to favorable interactions, including electrostatic attraction and chemisorption further confirmed by kinetics modelling. Due to the decrease in available active sites and the accumulation of fluoride on the surface, can lead to the formation of an adsorbate layer on the surface, which may act as a barrier to further adsorption by hindering the access of fluoride ions to the underlying active sites the adsorption gradually slowed down.

3.4.6 Kinetic study of fluoride adsorption

Adsorption kinetics of F^- on CeO_2/BC were further analysed by the pseudo-first-order [51] and pseudo-second-order kinetic model [52] by fitting the experimental data. Mathematical representations of these models are briefly given in Chapter 2 section **2.5.2**. The result of the fittings is presented in Fig. 3.5(b and c) and Table 3.2. According to Table 3.2, the pseudo-second-order kinetic model's R^2 values (0.99) were significantly higher than the pseudo-first-order kinetic model's R^2 values (0.69), and the adsorption capacity value $q_{e(calculated)}$ calculated from the pseudo-second-order kinetic model was more comparable with the experimental values $q_{e(experimental)}$. This demonstrates that the pseudo-second-order kinetic model predicts CeO_2/BC's ability to bind more accurately with F^- ions and remove them from water. The adsorption of fluoride on CeO_2/BC suggests that chemisorption is likely the cause of this. The entire process is dominated by the surface adsorption reaction, which is controlled by electrostatic forces. Similar results are found by Meng et al. 2022 [206].

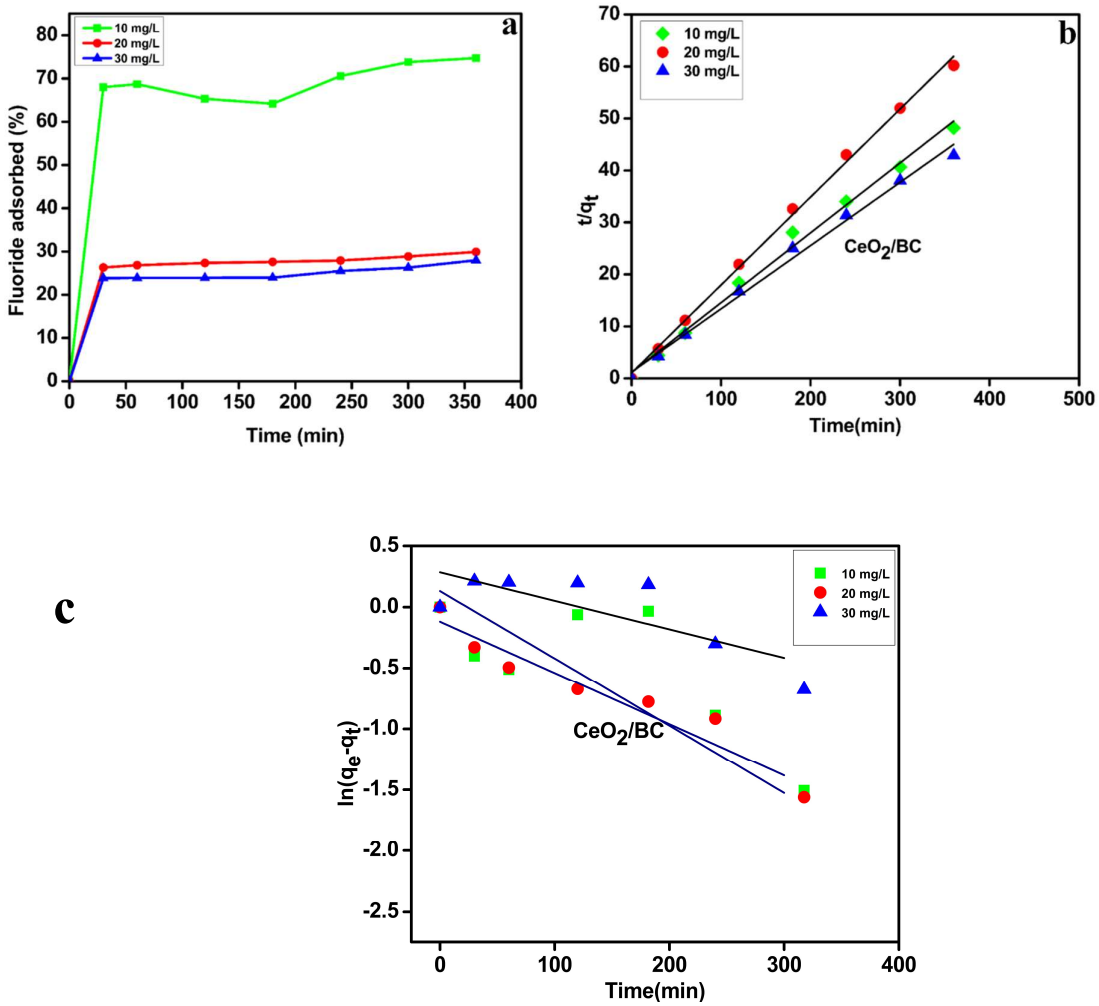

Fig. 3.5 (a) Effect of contact time on fluoride uptake by CeO_2/BC; (b) Plot of Pseudo-second-order kinetic model; (c) Pseudo-first-order kinetic plot of CeO_2/BC

Table 3.2: Different kinetic models' parameter for fluoride uptake by CeO_2/BC

C_0 (mg/L)	$q_{e(exp)}$ (mg/g)	Pseudo First Order			Pseudo Second Order		
		q_e (mg/g)	k_1 (min^{-1})	R^2	q_e (mg/g)	k_2 (min^{-1})	R^2
10	7.47	1.14	0.00	0.42	7.44	0.02	0.99
20	5.98	0.89	0.00	0.90	5.96	21.15	0.99
30	8.39	1.33	-0.00	0.50	8.22	55.55	0.99

3.4.7 Effect of initial concentration of fluoride on adsorption

It was noticed that before reaching equilibrium, the adsorbent's capacity to adsorb fluoride increases as fluoride concentration increases Fig. 3.6(a). This would be because higher fluoride concentrations make more fluoride ions available for adsorption, and since the active sites on the adsorbent surfaces become saturated, a plateau forms. Eventually, a point is reached where fluoride adsorption reaches maximum efficiency, and no further fluoride ions can be adsorbed.

3.4.8 Isotherm study of fluoride adsorption

The CeO_2/BC adsorption process is better described by the Langmuir, Freundlich, and Temkin isotherm models. The Langmuir model predicts single-layer adsorption [52] but neglects all other relationships between the adsorbate and adsorbent surface [53], whereas the Freundlich isotherm assumes multi-layer adsorption. The Temkin isotherm model [190] assumes that the uniform diffusion of binding energy can explain the linear reduction of adsorption heat. Mathematical representations of these models are briefly given in Chapter 2 section **2.5.3**.

When the experimental data fitted to the three isotherm models, namely Langmuir, Freundlich, and Temkin, were compared, as shown in Fig. 3.6 (b), (c) and (d) and Table 3.3, the Langmuir isotherm performed better than the other two. As a result, fluoride adsorption by CeO_2/BC can be better understood using the Langmuir isotherm. The Langmuir isotherm has advantages over other models as it assumes that the adsorbent surface comprises sites that can only accommodate one adsorbate molecule. The Langmuir isotherm calculates CeO_2/theoretical BC's maximum adsorption capacity to be 16.14 mg/g and explains that the adsorbent's adsorption was monolayer adsorption. Table 3.4 lists the adsorption capacities of few adsorbents used for fluoride uptake, which shows that CeO_2/BC has good fluoride uptake capacity.

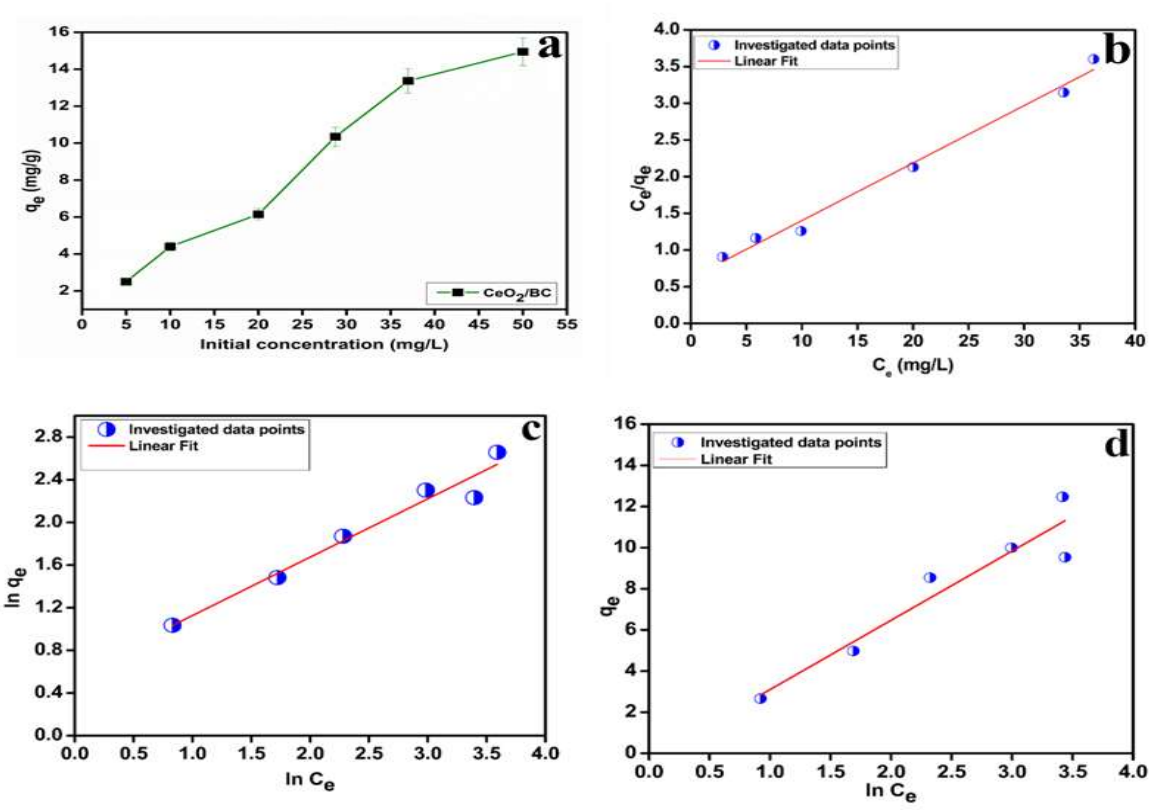

Fig. 3.6 (a) Effect of initial fluoride concentration on fluoride uptake by CeO_2/BC; (b) Langmuir, (c) Freundlich and (d) Temkin model of adsorption isotherm

Table 3.3: Different values of adsorption Isotherms for fluoride adsorption on CeO_2/BC

Isotherm models	Parameters	CeO_2/BC
Langmuir Isotherm	Q_0 (mg/g)	16.15
	b (L/mg)	206.23
	R^2	0.99
Freundlich Isotherm	K_F (mg/g)	3.79
	1/n	0.55
	R^2	0.95
Temkin Isotherm	K_T (L/g)	0.92
	B (J/mol)	3.37
	R^2	0.88

Table 3.4: List of known adsorbents used for defluoridation and their adsorption capacities

S. No.	Adsorbent	Adsorption capacity (mg/g)	pH	Time (min)	References
1	α-Fe_2O_3 and Fe_3O_4 dispersed on Douglas fir biochar	9	2–10	10	[207]
2	Vergin Musa paradisiaca (plantain pseudo-stem) modified carbons (VMPC)	11.4	2.04	60	[208]
3	ZrO_2 modified Camellia seed biochar	11.04	3–10	180	[204]
4	Iron modified yak dung biochar	3.94	5–6	1440	[209]
5	Corn stover biochar	6.42	2	60	[35]
6	Magnetic corn stover biochar	4.11	2	60	[35]
7	Gracilaria Rhodophyta biochar	2.1	6	90	[210]
8	Al modified Eucalyptus wood biochar	1.6	6	1440	[211]
9	CeO_2-Nanocubes	7	3	1500	[184]
10	cerium-loaded cellulose bead	2.35	3	60	[212]
11	CeO_2/BC	16.14	4-10	360	This work

3.4.9 Thermodynamic study of adsorbent CeO_2/BC

To further examine the adsorption process, the thermodynamic study of fluoride adsorption by CeO_2/BC was done and values are shown in Table 3.5. The measured ΔG° was negative at all temperatures (298 K to 308 K), showing that the reaction is spontaneously occurring and thermodynamically favorable. As the temperature was raised from 298 K to 308 K, the ΔG° values exhibited a decreasing trend, signifying that the adsorption capacity improved at elevated temperatures. The resultant ΔH° was positive, demonstrating the endothermic nature of fluoride adsorption on CeO_2/BC. Concurrently, the positive values of ΔS° signify an increasing disorderliness at the solid-liquid interface during the course of the fluoride adsorption process.

Table 3.5: Different values of thermodynamic parameters for fluoride adsorption by CeO_2/BC

Temperature (K)	ΔG° (kJ/mol)	ΔH° (kJ/mol)	ΔS° (kJ/mol K)
298	-0.40	17.93	61.30
303	-0.55		
308	-1.29		

3.5. REUSABILITY TEST

The findings of a reusability test after four cycles are shown in Fig 3.7. With each regeneration cycle, it was found that the CeO_2/BC adsorbent's adsorption capacity decreased, lowering its removal percentage. Even after the fourth cycle, this adsorbent is still effective at removing

fluoride. The amount it removes has, however, decreased by up to 20%, indicating that it can be used more than once, reducing cost and increasing feasibility. The reduction in removal capability after four cycles may be attributed to one of two factors. First, (i) extended use of the adsorbent results in the saturation of adsorption sites. With each adsorption-regeneration cycle, these sites become increasingly occupied by fluoride ions, making it difficult to fully desorb and regenerate the material. Alternatively, (ii) repeated exposure to the desorbing agent (NaOH) induces consequential structural modifications in the biochar matrix, including surface erosion and chemical transformations, as evident in SEM micrographs following adsorption Fig. 3.1 (c) and (d). These alterations can lead to a decrease in the number of available active sites, further limiting the regeneration capability.

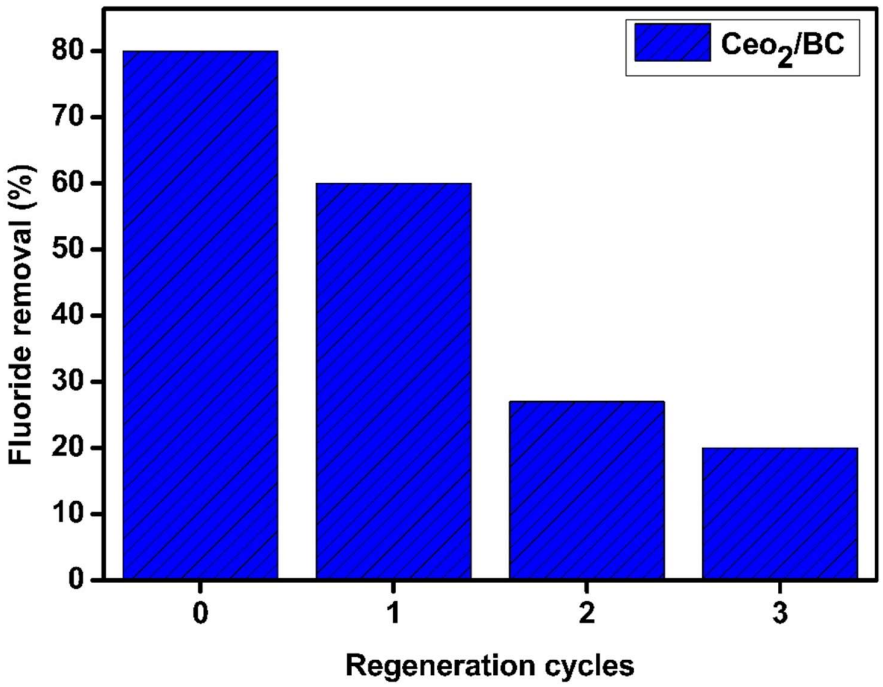

Fig. 3.7 Reusability cycle of CeO_2/BC biochar after regenerating with 0.5 M NaOH

3.6. ADSORPTION MECHANISM

Fig. 3.8 (a) show the full spectrum of the XPS survey spectrum, including binding energy peaks for F 1s, O 1s, and Ce 3 d, to compare the elementary composition before and after F^- adsorption by CeO_2/BC. The sorption of fluoride by CeO_2/BC resulted in the formation of a new F 1s peak, which may be due to CeF_3, which was clearly visible in the spectra Fig. 3.8 (b) [213,214]. The F 1s peak had a binding energy of 685.6 eV, which is more than the binding energy of pure NaF (684.6 eV) by 1.0 eV. The complexation reaction between Ce^{3+} and F^- is presumed to be responsible for the higher binding energy detected in CeO_2/BC than in NaF [214]. Three chemical interactions -O-C=O (288.8 eV), C-O (285.6 eV), and C-C (284.8 eV) bonding were revealed by the C 1s peak deconvolution Fig. 3.8 (e). This implies that functional groups like carboxyl, which are favourable for fluoride adsorption, are present in CeO_2/BC. The changes in O-H, Ce-OH, and Ce-O species were observed at binding energies of 532.1 eV, 531.5 eV, and 529.1 eV, respectively, and were observed using deconvolution of the O-1s peak Fig. 3.8(c). After adsorption, the O-H peak's position altered noticeably, and its area was significantly decreased, implying the participation of hydroxyl groups and perhaps an ion exchange of OH- with F^- [215]. Ce^{4+} and Ce^{3+} jointly contribute to Ce 3d's scan peak Fig. 3.8(d). Reduction in the peak area of Ce (IV) suggests that Ce (IV) is primarily responsible for the removal of fluoride, and a portion of Ce (IV) is converted to Ce (III) due to the high electro-negativity of the adsorbed fluoride [214]. This finding supports the formation of Ce-F inner-sphere complexation after fluoride intake onto CeO_2/BC. These results highlight the potential of CeO_2/BC as an efficient fluoride adsorbent in water treatment applications.

The pH_{zpc} results of CeO_2/BC revealed a pH_{zpc} value equal to 7. This finding indicates that the surface of CeO_2/BC becomes easily positively charged below pH 7. Owing to the protonation of the hydroxyl groups bonded to Cerium, the F^- anions in the solution are attracted

electrostatically to the surface of CeO_2/BC, thereby facilitating fluoride adsorption from the solution.

Based on the Hard-Soft-Acid-Base (HSAB) principle, Ce, a rare earth metal, is classified as a hard acid, while fluorine is a hard base [216]. As per the HSAB theory, the interaction between hard acids and hard bases results in an attraction but not neutralization, leading to the formation of stable complexes instead. Therefore, the rare earth metal Ce and F^- form stable complexes due to their mutual attraction, but no neutralization takes place.

Coupling pHzpc effect, the plausible mechanism of F^- removal by CeO_2/BC can be explained through three processes: (1) the electrostatic forces of attraction between the positively charged CeO_2/BC surface and the negatively charged fluoride ions; (2) the exchange of ligands amid hydroxyl groups of the CeO_2/BC and the F^- ions; (3) the creation of an inner-sphere complex between CeO_2/BC and fluoride, resulting in the formation of Ce-F bonds. These factors likely contribute to successfully eliminating fluoride through the CeO_2/BC adsorption mechanism. Based on all of the aforementioned analyses, the most feasible mechanisms for fluoride's adsorption onto RBM-Ce are expressed in. Based on all of the aforementioned analyses, the most feasible mechanisms for fluoride's adsorption onto CeO_2/BC are expressed in Fig. 3.9.

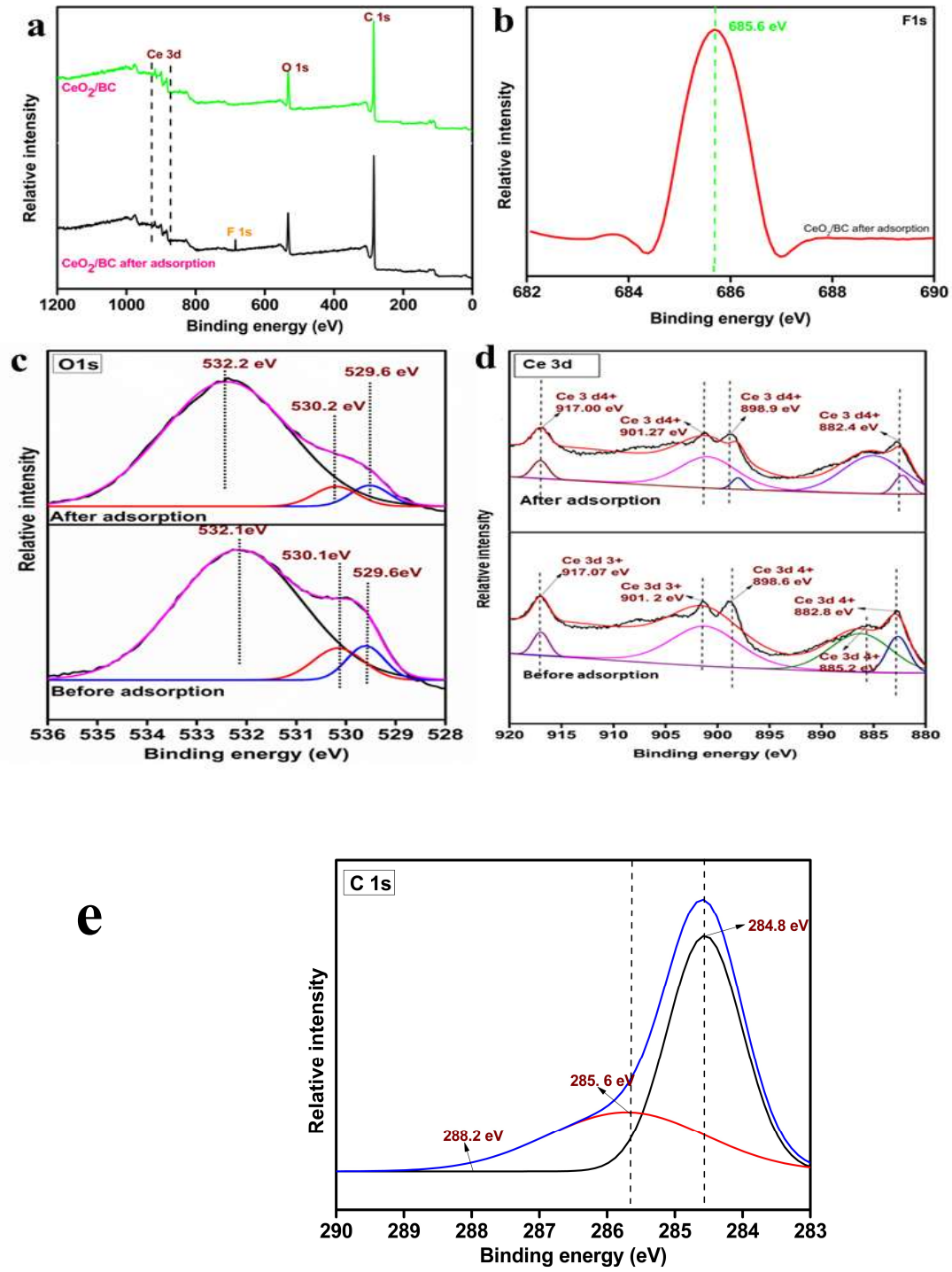

Fig. 3.8 XPS analysis results (a) XPS survey; (b) F 1s spectra after adsorption (c) O 1s spectra before and after adsorption; (d) Ce 3d spectra before and after adsorption; (e) C 1s XPS spectra of CeO_2/BC

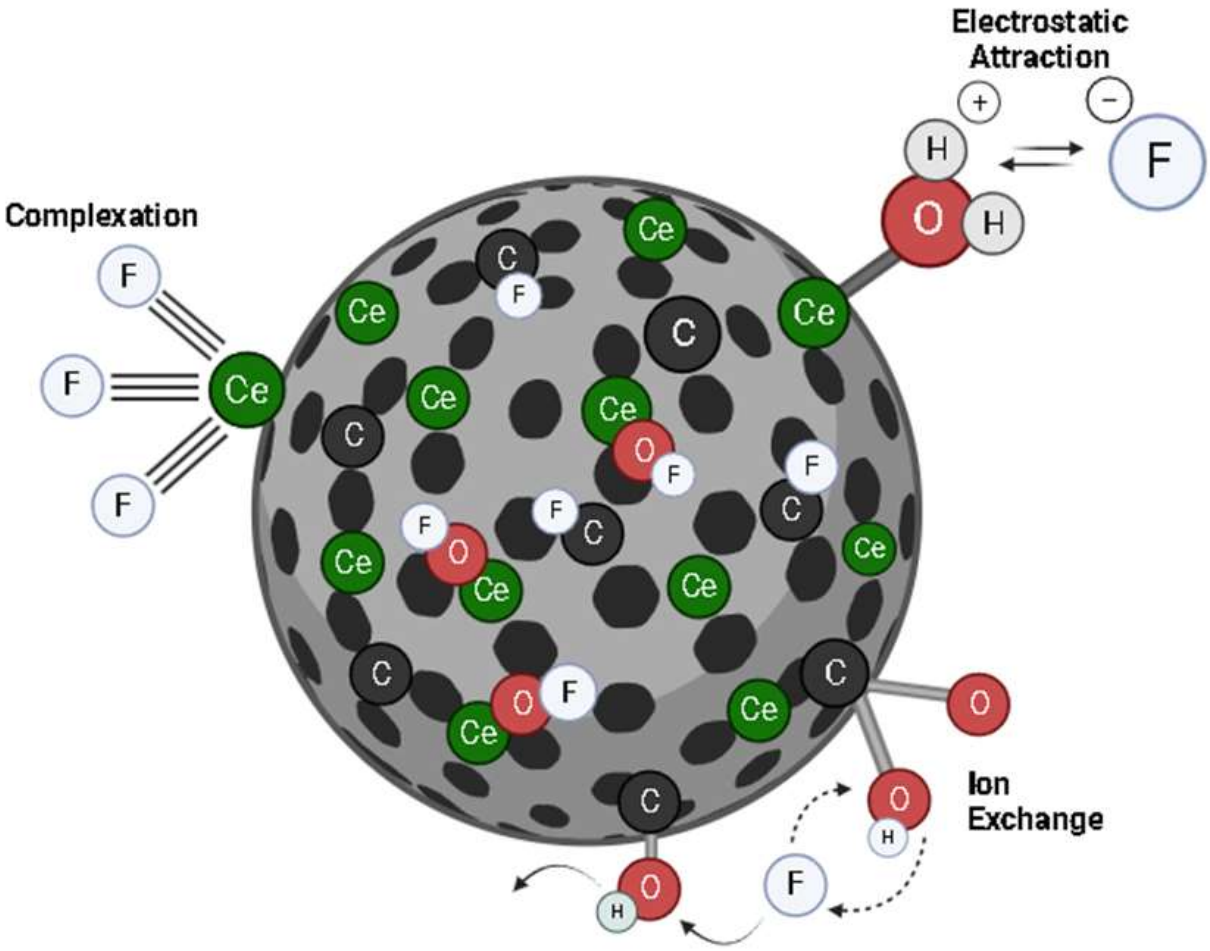

Fig. 3.9 Pictorial representation of the mechanism involved in fluoride adsorption by CeO_2/BC

3.7. CONCLUSION

For the elimination of F^- from water, the preparation of CeO_2-loaded biochar-based adsorbents was reported in this article. The chemical precipitation method shaped CeO_2/BC for F^- adsorption. It is energy efficient method as it involves biochar synthesis at 600 ºC and no further thermal treatment. It has been shown that adding 10 weight per cent CeO_2 significantly improves CeO_2/BC's ability to remove F^-. Batch experiments demonstrated that CeO_2/BC at a concentration of 2 g/L and a temperature of 25º C±1 could remove 69% fluoride in 30 minutes, displaying rapid removal. CeO_2/BC retained its adsorption capacity throughout the pH range of 4-10, removing 60% fluoride even at pH 10. Sorption of F^- is affected by the presence of HCO_3^- ion due to the dissolution of hydroxyl ion. The study also discovered that the adsorption process adhered to the Langmuir isotherm model, with a maximum theoretical adsorption capacity of 16.14 mg/g and the pseudo-second-order kinetic model. XPS, FTIR and pH_{ZPC} results show that the plausible mechanism of fluoride adsorption is electrostatic attraction, ion exchange and inner sphere complexation. This adsorbent also showed good reusability upto 4^{th} cycle, making it practical in use.

Using Cerium to engineer sugarcane biochar effortlessly makes it cost-effective and feasible for defluoridation. Cerium is reportedly used in many biomedical applications; hence it will not cause secondary health problems like Alzheimer's caused due to residual aluminium in treated water. Using sugarcane bagasse for biochar preparation is an efficient waste management step in areas where it is produced in large quantities.